Geoacoustic Inversion based on Covariance Weighted Bartlett Estimator

Zheng Zheng, Jingning Jiang and Xiang Pan*
College of Information Science and Electronic Engineering
Zhejiang University
Hangzhou, China, 310027
*Email: panxiang@zju.edu.cn

Abstract—**Bartlett estimator is a widely used objective function in matched field inversion (MFI) to quantify the misfit between measured acoustic field and replica field. In this paper, under the assumption of additive spatially correlated Gaussian residual errors, a normalized covariance weighted Bartlett estimator is employed in geoacoustic inversion as the objective function utilizing global optimization algorithm, differential evolution (DE). Both simulation and SW06 data are processed using this new weight-Bartlett strategy and the inversion results are compared with conventional Bartlett strategy. In the simulation, spatially colored Gaussian noise vectors are added to the generated pressure vectors. Using weight-Bartlett strategy, the estimated geoacoustic parameters including sediment thickness and sound speed of sediment and basement which are secondary sensitive to misfit function are closer to the true values than Bartlett strategy, leading to better inversion results. For source range and depth which are most sensitive to misfit function, both strategies achieve similar accurate results. While for parameters less sensitive to misfit function, offsets with respect to true values occur. For SW06 experimental data, the estimated geoacoustic parameters, e.g. sediment thickness and sound speed of sediment and basement of both strategies are consistent with other results at the same marine.**

Index Terms—**Geoacoustic inversion, differential evolution, covariance weighted Bartlett estimator.**

I. Introduction

In shallow water environments, adequate knowledge of geoacoustic parameters is essential to observe and predict the sound propagation. Geoacoustic parameters inversion is a highly nonlinear inverse problem with no analytical solution. Matched field inversion (MFI) is widely used to investigate the geoacoustic parameters and their uncertainties. Bayesian formulation has been a hot spot of MFI in acquiring solution to inversion problems. The solution is characterized by a posteriori probability distributions (PPD) of multi-dimension unknown parameters [1]. Fast Gibbs sampling [2, 3], and interacting Markov chains [4] are efficient sampling methods to estimate the moments and marginal probability distributions of these unknown parameters. While other work on MFI focused on developing global optimization algorithms to estimate the optimum geoacoustic parameters by minimizing the objective function which quantifies the misfit between the measured acoustic field and replica field [5–7]. Global optimization algorithm usually gives a fast convergence rate than that of Bayesian approach and fewer forward models are computed. Besides, the inversion results of global optimization can be also utilized as the initial values in Bayesian approach to accelerate the convergence rate.

The Bartlett estimator is a mostly used objective function in MFI. And the Bartlett estimator was derived from the assumption of addictive spatially uncorrelated Gaussian errors between array measured vectors and replica field vectors using maximum likelihood methods [8], so it's the optimum estimator when the residual errors are spatially uncorrelated between each sensor. Actually, the residual errors contain the model errors and underwater ambient noises, which are more likely to be spatially correlated. The influence of data errors statistics on the parameters' uncertainty estimation was investigated in [9, 10]. An autoregressive model (AR) to account for correlated errors has been proposed in [4, 11]. In this paper, the likelihood function for multi-snapshot broadband transmission signal is employed to acquire the normalized covariance weighted Bartlett estimator as the objective function in global optimization algorithm. As described in [9], estimation of covariance matrices of residual errors is by finite spatial averaging over the array measurements. Here, the covariance matrices of residual errors are estimated by both time-average and spatial-average.

The paper is organized as follows: Section II describes geoacoustic inversion problem, presents the derivation of covariance weighted Bartlett estimator and provides the brief introduction on differential evolution. Geoacoustic inversion strategies based on conventional Bartlett estimator and covariance weighted Bartlett estimator are referred to as Bartlett and weight-Bartlett strategy respectively. Section III applies both strategies to process simulation and SW06 data using differential evolution. The inversion results are compared. Section IV summarizes and discusses the work.

II. Theory

A. Geoacoustic inversion problems

Fig. 1 presents a shallow water waveguide model consists of water column, single- or multiple-layer sediment and semi-infinite basement. Geoacoustic parameters including water depth, sound speed profile, thickness h, sound speed c_1 and c_2, density ρ_1 and attenuation α_1 of sediment and sound speed c_b, density ρ_b and attenuation α_b of basement have great influence on sound propagation, which determine the performance of sonar systems.

978-0-933957-43-5 ©2015 MTS

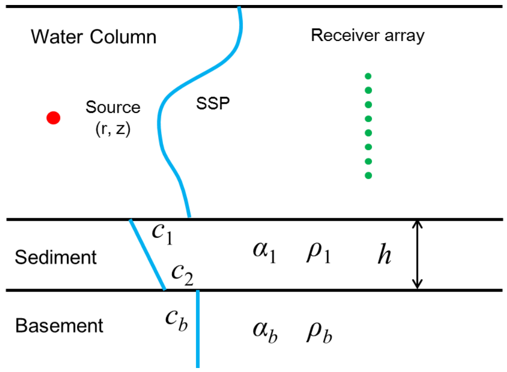

Fig. 1. Shallow water environment model

The source (range r and depth z) transmits narrow-band or broadband signals. The signals then propagate in underwater channel and are recorded by the receiver vertical or horizontal array. The received array signals contain the information of channel and source parameters. For broadband signal, the frequency band is discretized to several frequency bins, so multiple frequencies are employed to approximate the signal. For each frequency, we have several snapshots, where the number of snapshots is determined by the total received signals' duration and the correlation time of the source process. Source motion would limit the number of snapshots for calculating the covariance matrices of residual error vectors. So the source is assumed to be stationary. Also sound speed profile and other environment parameters' variations between different snapshots are neglected.

Suppose that we have T snapshots measurement data for K frequencies $f_k, k = 1, 2, \cdots, K$. The measurement function comes as,

$$\mathbf{y}(f_k, t) = S(f_k, t)\mathbf{h}(\mathbf{x}, f_k) + \mathbf{v}(f_k, t), \qquad t = 1, \cdots, T \quad (1)$$

where,

- $\mathbf{x}$ is the channel parameters including geoacoustic parameters and/or source localizations to be estimated;
- $\mathbf{y}(f_k, t)$ represents received data vectors, e.g. pressure vectors; The dimension of $\mathbf{y}(f_k, t)$ is N, which is the number of vertical or horizontal sensors;
- $S(f_k, t)$ donates the source strength which is generally unknown;
- $\mathbf{h}(\cdot)$ is the channel response function calculated by forward model, e.g. kraken, bellhop and etc;
- $\mathbf{v}(f_k, t)$ donates the array residual error vectors, $\mathbf{v}(f_k, t)$ contains measurement errors $\mathbf{v}^{ME}(f_k, t)$ and theoretic errors $\mathbf{v}^{TE}(f_k)$, that,

$$\mathbf{v}(f_k, t) = \mathbf{v}^{TE}(f_k) + \mathbf{v}^{ME}(f_k, t), \quad (2)$$
$$\mathbf{C}_k = E\{\mathbf{v}(f_k, t)\mathbf{v}^H(f_k, t)\} = \mathbf{C}_k^{TE} + \mathbf{C}_k^{ME}, \quad (3)$$

where $(\cdot)^H$ represents conjugate transpose, $\mathbf{C}_k$ is the covariance matrix of the array residual error vectors at frequency f_k and is assumed to be incoherent from frequency to frequency. The dimension of $\mathbf{v}(f_k, t)$ is N, so $\mathbf{C}_k$ is a $N \times N$ Hermitian matrix. Ocean ambient noises and array sensors' self-noise form the measurement errors, which are assumed to be time-varying and independent between different snapshots. Model errors such as simplification of environment model and approximation of parameters hold dominant position of theoretic errors, so the theoretic errors are generally not independent from snapshot to snapshot.

In the subsequent content, $\mathbf{y}_{k,t}$, $S_{k,t}$, $\mathbf{h}_k(\mathbf{x})$ and $\mathbf{v}_{k,t}$ are employed to represent $\mathbf{y}(f_k, t)$, $S(f_k, t)$, $\mathbf{h}(\mathbf{x}, f_k)$ and $\mathbf{v}(f_k, t)$ respectively for simplification.

B. Covariance weighted Bartlett estimator

Since we don't have prior information of the distribution of array residual errors, we assume the residual errors obey the zero-mean complex Gaussian probability density function (PDF) which is true for infinite snapshots according to the central limit theorem. A number of studies assume that the covariance matrix of array residual error vectors $\mathbf{C}_k$ to be diagonal, that is $\mathbf{C}_k = \sigma_k^2\mathbf{I}$, where σ_k^2 is the variance of residual errors on each sensor at frequency f_k. The zero values of diagonal covariance matrices mean that the residual errors are spatially uncorrelated. While we consider the residual errors to be spatially correlated due to the existence of theoretic errors and underwater ambient noises, that $\mathbf{C}_k$ has non-zero values in its off-diagonal entries.

Then, the likelihood function $L(\mathbf{x})$ can be expressed as,

$$L(\mathbf{x}) = \prod_{t=1}^{T}\prod_{k=1}^{K} \frac{1}{\pi^N \det(\mathbf{C}_k)} \exp\Big\{-\Big(\mathbf{y}_{k,t} - S_{k,t} \cdot \mathbf{h}_k(\mathbf{x})\Big)^H \mathbf{C}_k^{-1}\Big(\mathbf{y}_{k,t} - S_{k,t}\mathbf{h}_k(\mathbf{x})\Big)\Big\}, \quad (4)$$

where, $\det(\cdot)$ denotes determinant of a square matrix. Since $S_{k,t}$ is generally unknown, it's estimated according to maximum likelihood principles. Take derivation of $L(\mathbf{x})$ with respect to conjugate of $S_{k,t}$, that is $\partial L(\mathbf{x})/\partial S_{k,t}^*$, and set it equals to 0 leading to,

$$\hat{S}_{k,t} = \frac{\mathbf{h}_k^H(\mathbf{x})\mathbf{C}_k^{-1}\mathbf{y}_{k,t}}{\mathbf{h}_k^H(\mathbf{x})\mathbf{C}_k^{-1}\mathbf{h}_k(\mathbf{x})}, \quad (5)$$

and thus, the likelihood function is,

$$L(\mathbf{x}) = \prod_{t=1}^{T}\prod_{k=1}^{K} \frac{1}{\pi^N \det(\mathbf{C}_k)} \exp\{-B_{k,t}(\mathbf{x})\}, \quad (6)$$

where $B_{k,t}(\mathbf{x})$ is the covariance weighted Bartlett mismatch as,

$$B_{k,t}(\mathbf{x}) = \mathbf{y}_{k,t}^H\mathbf{C}_k^{-1}\mathbf{y}_{k,t} - \frac{\left|\mathbf{h}_k^H(\mathbf{x})\mathbf{C}_k^{-1}\mathbf{y}_{k,t}\right|^2}{\mathbf{h}_k^H(\mathbf{x})\mathbf{C}_k^{-1}\mathbf{h}_k(\mathbf{x})}. \quad (7)$$

Take the normalization form of Eq. (7) gives,

$$E(\mathbf{x}) = 1 - \frac{1}{KT}\sum_{k=1}^{K}\sum_{t=1}^{T}\left|\mathbf{h}_k^H(\mathbf{x})\mathbf{C}_k^{-1}\mathbf{y}_{k,t}\right|^2 \Big/ \Big(\left|\mathbf{h}_k^H(\mathbf{x})\mathbf{C}_k^{-1}\mathbf{h}_k(\mathbf{x})\right| \cdot \left|\mathbf{y}_{k,t}^H\mathbf{C}_k^{-1}\mathbf{y}_{k,t}\right|\Big), \quad (8)$$

which is defined as covariance-weighted Bartlett estimator of data with T snapshots and K frequencies, where $E(\mathbf{x})$ approaches 0 means forward model vectors sets $\{\mathbf{h}_k(\mathbf{x}), k = 1, \cdots, K\}$ match well with measured data vectors sets $\{\mathbf{y}_{k,t}, k = 1, \cdots, K, t = 1, \cdots, T\}$.

We note that, when residual errors are spatially white, that is $\mathbf{C}_k = \sigma_k^2\mathbf{I}$, Eq. (8) simplifies to,

$$E(\mathbf{x}) = 1 - \frac{1}{KT}\sum_{k=1}^{K}\sum_{t=1}^{T}\frac{\left|\mathbf{h}_k^H(\mathbf{x})\mathbf{y}_{k,t}\right|^2}{\left|\mathbf{h}_k^H(\mathbf{x})\mathbf{h}_k(\mathbf{x})\right| \cdot \left|\mathbf{y}_{k,t}^H\mathbf{y}_{k,t}\right|}, \quad (9)$$

which is the classical Bartlett estimator used in MFI.

C. Wight-Bartlett strategy

Eq. (8) needs the knowledge of covariance matrix $\mathbf{C}_k$, which is hardly acquired in practice. In [9, 10], the error process was assumed to be stationary and ergodic, so $\mathbf{C}_k$ can be estimated by finite spatial average. In this paper, we adopt both time average and spatial average to estimate the covariance matrix $\mathbf{C}_k$.

Firstly, $\mathbf{x}$ is estimated by minimization of Eq. (9), donated by $\hat{\mathbf{x}}$. The data residual errors are,

$$\mathbf{v}_{k,t} = \mathbf{y}_{k,t} - \hat{S}_{k,t}\mathbf{h}_k(\hat{\mathbf{x}}). \quad (10)$$

And the (i,j)th entry of $\mathbf{C}_k$ is

$$\left\{\hat{\mathbf{C}}_k\right\}_{ij} = \begin{cases} \frac{1}{NT}\sum_{t=1}^{T}\sum_{n=1}^{N-|i-j|}\left(\{v_{k,t}\}_n - \overline{v}_k\right)^* & \\ \quad\cdot\left(\{v_{k,t}\}_{n+|i-j|} - \overline{v}_k\right), & i \geq j; \\ \mathbf{C}_{k,ji}^*, & i < j. \end{cases} \quad (11)$$

where $\overline{v}_k$ is the mean value of $\mathbf{v}_k$ at f_k, subtracting $\overline{v}_k$ ensures that residual error vectors are zero-mean vectors.

Once $\hat{\mathbf{C}}_k$ is estimated, the global optimization algorithm is employed to estimate a new vector $\hat{\mathbf{x}}$ by minimization of Eq. (8). So the process is repeated until both unknown parameters $\hat{\mathbf{x}}$ and $\hat{\mathbf{C}}_k$ converge to final values. The strategy refers to weight-Bartlett strategy. And correspondingly, geoacoustic inversion strategy based on the objective function of Eq. (9) refers to Bartlett strategy.

D. Global optimization algorithm

Global optimization algorithms such as genetic algorithm and simulated annealing have been employed in MFI by minimizing the objective function (e.g. Eq. (9)). In [5], different optimization algorithms employed in inversion were compared.

In this paper, differential evolution (DE) [6, 12] is adopted to investigate the geoacoustic parameters utilizing the objective function of Eq. (8) and (9), that is weight-Bartlett strategy and Bartlett strategy respectively. DE can handle multidimensional real-valued nonlinear functions and fast convergence rate is guaranteed by the use of DE. Details on DE can be found in [12].

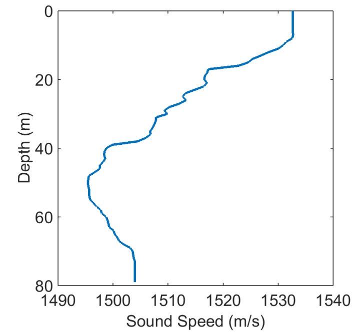

Fig. 2. Sound speed profile used in both simulation and SW06 experimental data

III. Inversion Examples

In this section, both Bartlett and weight-Bartlett strategies are employed to process simulation and SW06 data and the results are compared. Fig. 1 is a widely used underwater environment model. So the model is employed both in simulation and SW06 data.

A. Simulations

The true geoacoustic parameters in simulation are listed in Table I. And the search bounds of geoacoustic parameters and source localizations are also shown in Table I.

In the simulation, received array pressure vectors are computed using kraken with the given environment parameters. Colored zero-mean Gaussian noise vectors with $SNR = 10dB$ of $T = 20$ snapshots are added to the generated pressure vectors as the residual error vectors. The covariance matrix of the residual error vectors is generated by AR(1) model ($a = 0.5$) so the off-diagonal values of $\mathbf{C}_k$ are not zero. And the normalized values of real parts of covariance matrix are shown in Fig. 3(a) (here, the same covariance matrices are adopted for different frequencies). The cross correlations between adjacent elements are strong and with spatial space increases, the correlations decrease, which is expected in practice. The imaginary parts of covariance matrix are 0 so the cross correlations between real and imaginary parts of pressure vectors are 0.

The parameters of DE algorithm are: population is 100, mutation weighting factor is 0.8, crossover probability is 0.5, and the maximum iterations in Bartlett strategy is 1000.

When employing weight-Bartlett strategy the geoacoustic parameters $\mathbf{x}$ and covariance matrices $\mathbf{C}_k$ are both estimated. Firstly, $\hat{\mathbf{x}}$ is estimated by minimization Eq. (9), that is Bartlett strategy. We use 300 iterations to estimate the first $\hat{\mathbf{x}}$, and $\hat{\mathbf{C}}_k$ is calculated by Eq. (11). After the first 300 iterations, we expect the $\hat{\mathbf{x}}$ to be close to the true values, and then the covariance matricces of residual error vectors are re-estimated every 100 iterations. The maximum iterations used in weight-Bartlett strategy is also 1000.

The curves of objective functions using Bartlett and weight-Bartlett strategies are shown in Fig. 4. The misfit function of Bartlett strategy converges to 0.0859 after about 200 iterations,

TABLE I
SIMULATION PARAMETERS AND INVERSION RESULTS OF THE TWO STRATEGIES

Type	Parameters	True values	Search bounds	Bartlett strategy	Weight-Bartlett strategy
Geoacoustic parameters	$h(m)$	20	$[10, 50]$	19.53	20.03
	$c_1(m/s)$	1620	$[1500, 1700]$	1621.1	1614.8
	$c_2(m/s)$	1650	$[1500, 1700]$	1656.5	1655.0
	$\rho_1(g/cm^3)$	1.6	$[1.2, 2.0]$	1.600	1.572
	$\alpha_1(dB/\lambda)$	0.35	$[0.01, 0.5]$	0.370	0.340
	$c_b(m/s)$	1740	$[1600, 1900]$	1787.9	1805.2
	$\rho_b(g/cm^3)$	2.0	$[1.2, 3.0]$	2.317	2.937
	$\alpha_b(dB/\lambda)$	0.765	$[0.01, 1.0]$	0.035	0.408
Water column	water depth(m)	79	–	–	–
	SSP	Fig. 2	–	–	–
Source localizations	$r(km)$	2.0	$[0.5, 5]$	1.998	2.002
	$z(m)$	30	$[5, 75]$	30.07	29.86
	frequency (Hz)	203,253	–	–	–
Receiver array	N	16	–	–	–
	elements' depths(m)	$[14.55 : 3.75 : 70.8]$	–	–	–

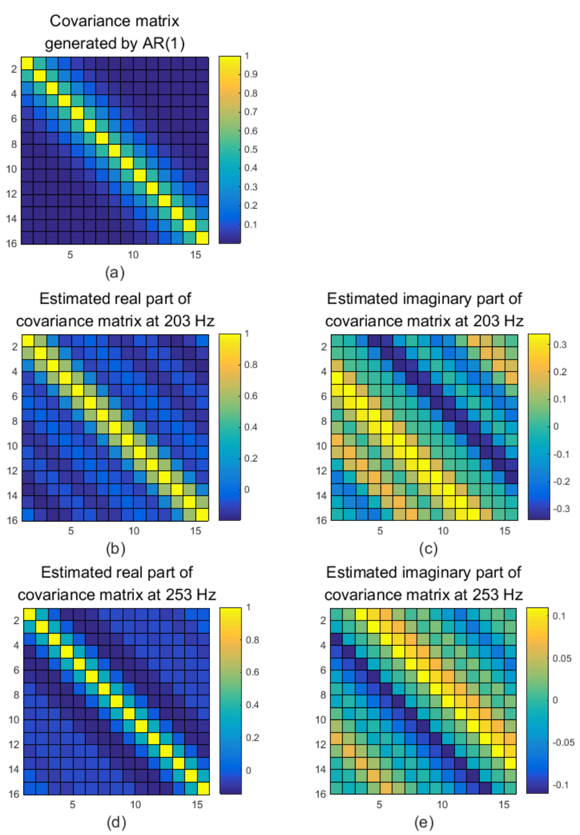

Fig. 3. Covariance matrix generated by AR(1) and estimated Hermitian covariance matrices at 203 and 253 Hz by weight-Bartlett strategy

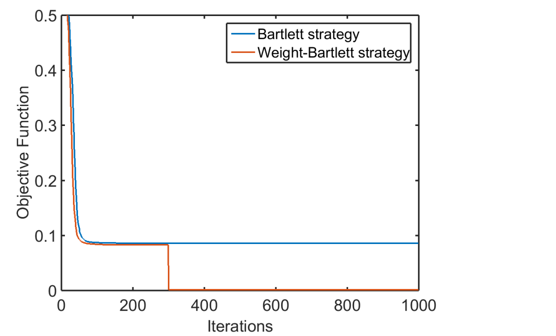

Fig. 4. Objective functions of Bartlett strategy (blue) and weight-Bartlett strategy (red) in simulation

which shows the fast convergence rate of DE algorithm. The misfit functions of the two strategies coincide well of the first 300 iterations. For weight-Bartlett strategy, the covariance matrices of residual error vectors are estimated after 300 iterations. The objective function is revised as Eq. (8). Due to spatially correlated residual error vectors, Eq. (8) is a better misfit function than Eq. (9). So the misfit declines rapidly after covariance estimated and finally the misfit converges to 0.0017. Fig. 3(b)$\sim$(e) also shows the estimated Hermitian covariance matrices at 203 and 253 Hz by weight-Bartlett strategy. The real parts of the estimated Hermitian covariance matrices coincide well with the generated covariance matrix, especially at $253Hz$. But the estimated covariance matrices also contain imaginary parts with values close to 0. The estimated covariance matrices show the validity of weight-Bartlett strategy and DE algorithm.

The marginal probability distributions of parameters represented by the last population of DE algorithm using Bartlett strategy and weight-Bartlett strategy are shown in Fig. 5. The source localizations including source range and depth are most sensitive to the misfit function. And the estimated source range and depth coincide well with true values with both strategies. For sediment thickness h and sound speed c_1, c_2 and sound speed of bottom c_b, which are secondary sensitive to the misfit function, the estimated parameters' values are close to the true values. The parameters computed by weight-Bartlett strategy are closer to the true values except sediment top sound speed c_1. The density and attenuation, especially those of bottom, are less sensitive geoacoustic parameters. So of course these parameters have less influence on misfit function, and the estimated parameters deviated from the true values of both strategies. It has been mentioned in [9] that using Bartlett strategy, the off-diagonal elements of covariance

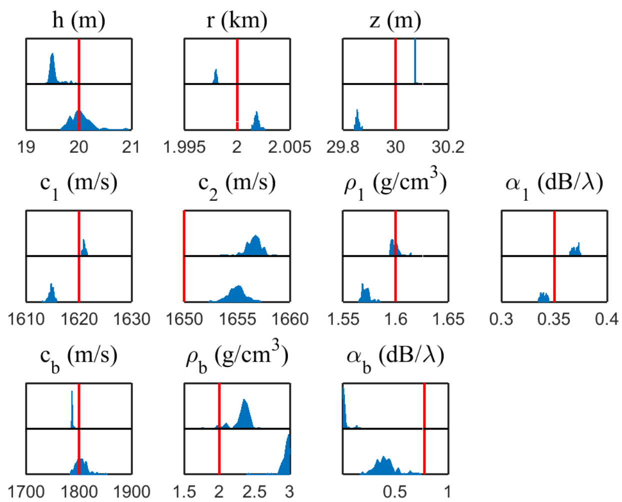

Fig. 5. Marginal probability distributions of parameters represented by the last population of DE algorithm of simulation using Bartlett strategy (top) and weight-Bartlett strategy (bottom), red lines indicate true values

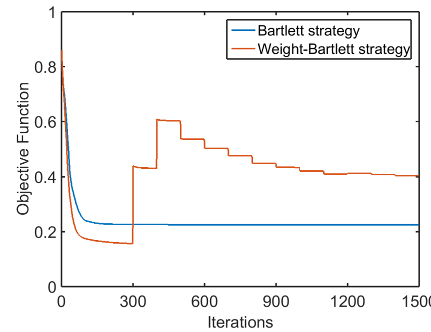

Fig. 6. Objective functions of Bartlett strategy (blue) and weight-Bartlett strategy (red)

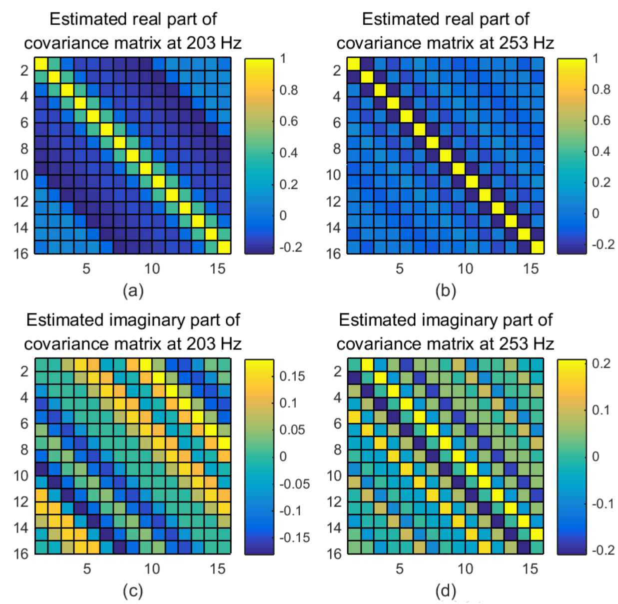

Fig. 7. Covariance matrix generated by AR(1) and estimated Hermitian covariance matrices at 203 and 253 Hz by weight-Bartlett strategy

matrices have been neglected, so it leads to narrower marginal probability distributions than the actual distributions. The marginal probability distributions of weight-Bartlett are wider than that of Bartlett strategy for some parameters, which has verified the conclusion.

B. SW06 data

In summer 2006, a series of Shallow Water Experiments (SW06) were carried out in shallow water near the shelf break on the New Jersey continental shelf [13]. The low frequency (LF, with frequencies of $53, 103, 203, 253Hz$) experimental data were recorded on Aug. 25, 2006 at $(39°01.477'N,\ 73°02.256'W)$ by a vertical line array (VLA) with elements' depthes listed in Table I. The VLA was located in the center of a $1km^2$ area for the LF acoustic experiments studies. The vicinity of the experimental sites has been extensively surveyed previously, and also during SW06. A distinguishing feature of the ocean bottom at the SW06 site is a ubiquitous subsurface seismic "R"-reflector [7]. There is also an erosional channel above the "R"-reflector in some of the area. In this part, the inversion results of SW06 LF experimental data are presented (experimental data at 203 and $253Hz$ are used).

The search bounds of geoacoustic parameters are the same as table I and the sound speed profile adopted in inversion is shown in Fig. 2. For source localizations, the search bounds are revised as $[0.1, 2]$ and $[10, 50]$ for r and z respectively. And in order to guarantee that both strategies converge, the maximum iterations is justified to 1500.

Fig. 6 shows the curves of objective functions using Bartlett and weight-Bartlett strategies. Alike the curves in simulation, Bartlett strategy converged after about 200 iterations. But unfortunately, the misfit rises after the covariance matrices estimated in the weight-Bartlett strategy. Afterwards, the misfit declines as several new covariance matrices estimated and ultimately, the misfit converged to 0.404. This large misfit value occurs largely due to non perfect estimation of covariance matrices. In Section II-C, we assume that array elements' residual errors have equal variances and cross correlations. But theoretic errors may be more complicated than the assumption and harder to formulate and estimate. Fig. 7(a)∼(d) shows the estimated Hermitian covariance matrices at 203 and 253 Hz by weight-Bartlett strategy. The estimated residual errors at $203Hz$ have stronger spatial cross correlations between adjacent sensors than at $253Hz$. And the cross correlations decrease as spatial space increases. The imaginary parts of covariance matrices are also round 0, which shows that weak correlations between real and imaginary parts of residual error vectors.

Fig. 8 shows the marginal probability distributions of geoacoustic parameters and source localizations represented by the last population of DE algorithm using Bartlett strategy and weight-Bartlett strategy. For parameters most sensitive

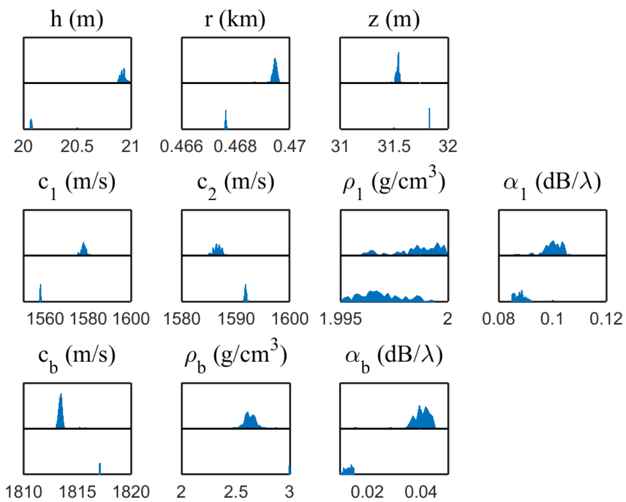

Fig. 8. Marginal probability distributions of parameters represented by the last population of DE algorithm of SW06 data using Bartlett strategy (top) and weight-Bartlett strategy (bottom), red lines indicate true values

and secondary sensitive to misfit function, the estimated parameters by both strategies are very close. The inversion results of SW06 experimental data are listed in Table II. The estimated thickness and sound speed of sediment and sound speed of bottom using both strategies are consistent with other results at the same marine, with a $\sim 20m$-thick sediment layer with sound speed of around $\sim$ 1600 m/s over a hard basement whose sound speed is approximately $\sim$ 1800 m/s[7]. For source localizations which are most sensitive to misfit function, the inversion results are expected to be most precise.

TABLE II
INVERSION RESULTS OF SW06 DATA USING THE TWO STRATEGIES

Parameters	Bartlett strategy	Weight-Bartlett strategy
$h(m)$	20.92	20.07
$c_1(m/s)$	1578.0	1558.0
$c_2(m/s)$	1586.6	1591.8
$\rho_1(g/cm^3)$	1.999	1.997
$\alpha_1(dB/\lambda)$	0.100	0.088
$c_b(m/s)$	1813.5	1817.1
$\rho_b(g/cm^3)$	2.634	2.998
$\alpha_b(dB/\lambda)$	0.040	0.013
$r(km)$	0.469	0.467
$z(m)$	31.53	31.83

IV. CONCLUSION

In the paper, simulation and SW06 data are processed using Bartlett strategy and weight-Bartlett strategy using DE algorithm and inversion results are compared.

In the simulation, zero-mean Gaussian distributed and spatially correlated residual error vectors are added to original simulated received pressure vectors. Utilizing the weight-Bartlett strategy, the misfit converges to $\sim 10^{-3}$, much smaller than that of Bartlett strategy. Using the weight-Bartlett strategy, the estimated geoacoustic parameters including sediment thickness and sound speed and bottom sound speed which are secondary sensitive to misfit function, are closer to the true values, and hence better inversion results. For parameters most sensitive to misfit function, e.g., source range and depth, both strategies achieve similar accurate results. While for parameters less sensitive to misfit function, e.g., densities and attenuations of sediment and bottom, both strategies encounter big offsets with respect to true values.

For SW06 experimental data, the misfit between measured field and replica field rises after the covariance matrices first estimated in the weight-Bartlett strategy. Afterwards, the misfit declines and finally converged to 0.404. The inversion results of SW06, including sediment thickness, sound speed of sediment and bottom are consistent with the results at the same marine. The inversion results of SW06 data show the validity of weight-Bartlett strategy in MFI.

In the paper, the distribution of array residual errors is assumed to be zero-mean correlated complex Gaussian distribution, and the covariance matrices are assumed to be Hermitian and Toeplitz. In MFI, a simplified environment model is used to approximate the real environments, which refers to theoretic errors. Due to the existence of theoretic errors, it's complicated to model the residual errors between measured field and replica field. The theoretic errors may lead to non Toeplitz property of covariance matrices, e.g, uneven diagonal elements, unequal off-diagonal elements and etc. So the estimated covariance matrices are not perfect and need to be modified further.

ACKNOWLEDGMENT

The paper is supported by the National Natural Science Foundation of China (No. 61171148). The authors would like to thank Dr. N. R. Chapman for the SW06 experimental data.

REFERENCES

[1] P. Gerstoft and C. F. Mecklenbräuker, "Ocean acoustic inversion with estimation of a posteriori probability distributions," *J. Acoust. Soc. Amer.*, vol. 104, no. 2, pp. 808–819, 1998.

[2] S. E. Dosso, "Quantifying uncertainty in geoacoustic inversion. i. a fast gibbs sampler approach," *J. Acoust. Soc. Amer.*, vol. 111, no. 1, pp. 129–142, 2002.

[3] S. E. Dosso and P. L. Nielsen, "Quantifying uncertainty in geoacoustic inversion. ii. application to broadband, shallow-water data," *J. Acoust. Soc. Amer.*, vol. 111, no. 1, pp. 143–159, 2002.

[4] J. Dettmer and S. E. Dosso, "Trans-dimensional matched-field geoacoustic inversion with hierarchical error models and interacting markov chains," *J. Acoust. Soc. Amer.*, vol. 132, no. 4, pp. 2239–2250, 2012.

[5] M. R. Fallat and S. E. Dosso, "Geoacoustic inversion via local, global, and hybrid algorithms," *J. Acoust. Soc. Amer.*, vol. 105, no. 6, pp. 3219–3230, 1999.

[6] M. Snellen and D. G. Simons, "An assessment of the performance of global optimization methods for geoacoustic inversion," *J. Comput. Acoust.*, vol. 16, no. 02, pp. 199–223, 2008.

[7] Y. M. Jiang, N. Chapman, and P. Gerstoft, “Estimation of geoacoustic properties of marine sediment using a hybrid differential evolution inversion method,” *IEEE J. Ocean. Eng.*, vol. 35, no. 1, pp. 59–69, 2010.

[8] C. F. Mecklenbräuker and P. Gerstoft, “Objective functions for ocean acoustic inversion derived by likelihood methods,” *J. Comput. Acoust.*, vol. 8, no. 02, pp. 259–270, 2000.

[9] S. E. Dosso, P. L. Nielsen, and M. J. Wilmut, “Data error covariance in matched-field geoacoustic inversion,” *J. Acoust. Soc. Amer.*, vol. 119, no. 1, pp. 208–219, 2006.

[10] H. Dong and S. E. Dosso, “Bayesian inversion of interface-wave dispersion for seabed shear-wave speed profiles,” *IEEE J. Ocean. Eng.*, vol. 36, no. 1, pp. 1–11, 2011.

[11] J. Dettmer, S. Molnar, G. Steininger, S. E. Dosso, and J. F. Cassidy, “Trans-dimensional inversion of microtremor array dispersion data with hierarchical autoregressive error models,” *Geophys. J. Int.*, vol. 188, no. 2, pp. 719–734, 2012.

[12] R. Storn and K. Price, “Differential evolution–a simple and efficient heuristic for global optimization over continuous spaces,” *J. Global Optim.*, vol. 11, no. 4, pp. 341–359, 1997.

[13] D. Tang, J. N. Moum, J. F. Lynch, P. A. Abbot, R. Chapman, P. H. Dahl, T. F. Duda, G. G. Gawarkiewicz, S. M. Glenn, J. A. Goff, *et al.*, “Shallow water06: A joint acoustic propagation/nonlinear internal wave physics experiment,” 2007.